Spin dynamics in $S=3/2$ one-dimensional Heisenberg antiferromagnets $CsVCl_3$ and $CsVBr_3$

Shinichi Itoh
Neutron Science Laboratory, Institute of Materials Structure Science, High Energy Accelerator Research Organization, Tsukuba 305-0801, Japan

Yasuo Endoh
Physics Department, Graduate School of Science, Tohoku University, Sendai 980-8578, Japan

Kazuhisa Kakurai
Neutron Scattering Laboratory, Institute for Solid State Physics, University of Tokyo, Tokai 319-1106, Japan

Hidekazu Tanaka
Department of Physics, Faculty of Science, Tokyo Institute of Technology, Tokyo 152-8551, Japan

Steve M. Bennington and Toby G. Perring
ISIS Facility, Rutherford Appleton Laboratory, Chilton, Didcot, Oxon OX11 0QX, United Kingdom

Kenji Ohoyama
Institute for Materials Research, Tohoku University, Sendai 980-8577, Japan

Mark J. Harris
ISIS Facility, Rutherford Appleton Laboratory, Chilton, Didcot, Oxon OX11 0QX, United Kingdom

Kenji Nakajima
Neutron Scattering Laboratory, Institute for Solid State Physics, University of Tokyo, Tokai 319-1106, Japan

Chris D. Frost
ISIS Facility, Rutherford Appleton Laboratory, Chilton, Didcot, Oxon OX11 0QX, United Kingdom
(Received 14 December 1998)

The spin dynamics in $S=3/2$, one-dimensional (1D) Heisenberg antiferromagnets, $CsVCl_3$ and $CsVBr_3$, was investigated using inelastic neutron scattering. The magnetic excitations were measured at temperatures above the three-dimensional ordering temperature in order to discuss the 1D properties in the present systems. We report on the spin dynamics at low temperatures and its temperature (T) dependence. From the observed dispersion relation, using the renormalization constant calculated from the quantum Monte Carlo method, we obtained the exchange constant (J) in good agreement with those taken from bulk-susceptibility measurements. The observed structure factor was well described by that calculated from the parameters describing the dispersion relation. The energy width (Γ) was independent of the 1D momentum transfer (q) at large energy transfers, however, its q dependence exhibits the minimum at the magnetic zone center. The parameters describing the energy scale in the spin dynamics at low T were found to be scaled by J. We also investigated the T dependence of the spin dynamics: $\Gamma(T)$ can be scaled by J, $\Gamma(T)$ at $T>J$ is proportional to T as predicted by classical theory but at $T>J$, Γ decreases with decreasing T and becomes finite. On the other hand, we found that $\kappa(T)$ is proportional to T at any T. The scaling by J in the dynamics at low T as well as $\Gamma(T)$ suggests that the observed spin dynamics is of 1D origin. We conclude that the spin dynamics at high temperatures $T>J$, is well described by classical theory, however, at low temperatures $T<J$, the finite width indicates some quantum fluctuations. Therefore, we observed the crossover from the quantum state at low T to the classical state at high T in $S=3/2$ systems. [S0163-1829(99)00521-4]

I. INTRODUCTION

The spin dynamics in one-dimensional (1D) Heisenberg antiferromagnetic systems is understood to be strongly dependent on the spin value (S). Quantum effects in the spin dynamics in a system with a small spin value ($S=1/2$ and 1) have been intensively studied both theoretically and experimentally. For an $S=1/2$ system, many important features have been theoretically proposed: the Néel state is not the ground state,[1] there is a quantum renormalization such that the excitation energy is $\pi/2$ times as large as that in a classical system,[2] the spin-wave-like dispersion curve is the lower boundary of an excitation continuum,[3] and so on. These features have been experimentally confirmed in real materials.[4,5] Since the spin-value-dependent dynamics was predicted, i.e., half-integer spin systems show gapless excitations and power-law decay in the spin correlations, and integer spin systems show an excitation gap and exponentially decaying correlations,[6] the dynamical properties in $S=1$ systems have been intensively investigated, and the Haldane effect was confirmed.

On the other hand, neutron-scattering experiments from tetramethylammonium manganese chloride have revealed that an $S=5/2$ system behaves classically.[7] A classical system exhibits ordering at absolute zero, and dynamical scaling can be applied to the phase transition.[8,9] Classical theory[10] has predicted that the energy width (Γ) of the magnetic excitations is independent of the 1D momentum transfer (q) and is proportional to the inverse correlation length (κ) at low temperatures; these behaviors are consistent with the dynamical scaling. As a result of the linear temperature (T) dependence of κ,[11] Γ should then be proportional to T.

Since a real system is a quasi-1D system, it exhibits a three-dimensional (3D) ordering at a finite temperature (T_N: 3D ordering temperature) due to the finite interchain interaction (J'). In order to discuss one-dimensionality in a real system, investigations of the dynamical properties at temperatures higher than T_N, where the properties in the 3D ordered state should be negligible, is required; also, the above-mentioned spin dynamics in $S=1/2$, 1 and 5/2 systems has been confirmed experimentally at temperatures well above T_N. Recent numerical studies have concentrated on investigations of an $S=2$ system,[12,13] which should exhibit the Haldane effect with the next integer spin to $S=1$. However, in a real $S=2$ system the temperature range where the system shows the quantum effect is expected to be much lower than T_N.[13] In fact, it has been reported, using inelastic neutron scattering, that an $S=2$ system, $CsCrCl_3$, behaves classically above $T_N(=16\,\mathrm{K})$.[14] Therefore, one might observe a crossover from the quantum to the classical limit at around $S=3/2$ with a real system, and we have initiated experiments to investigate the spin dynamics in an $S=3/2$ system, mainly using pulsed neutron scattering.[15–19]

$CsVCl_3$ is a compound recognized as an excellent realization of an $S=3/2$ system above $T_N=13.3\,\mathrm{K}$.[20] The intrachain exchange constant (J) was evaluated to be 115 K from bulk-susceptibility measurements.[21] Inelastic neutron measurements on this compound using a triple-axis spectrometer installed at a steady-state neutron source has been reported, and, from the determination of the spin-wave-dispersion relation well below T_N, the ratio $|J'/J|$ was estimated to be on the order of 10^{-4}.[22–24] The excitation energies in the interchain dispersion observed well below T_N reduce with the temperatures approaching T_N, and eventually, excitations from the interchain dispersion are not observed at finite energy transfers at temperatures above T_N. Therefore, the magnetic excitations in finite energy transfers at temperatures above T_N are considered to reflect only the 1D properties. In our previous experiments, using a chopper spectrometer installed at a pulsed spallation neutron source, at a low temperature ($T=40\,\mathrm{K}$) above T_N (=13.3 K), we found that Γ is independent of q, as predicted by classical theory, but is broader than the classical estimation.[16,17] The zone-boundary energy was determined to be 75 meV.[16] Measuring the T dependence of Γ, based on the assumption of the q-independent Γ, we also found that the observed Γ decreases as T decreases, but becomes almost constant and finite at low T.[18] This behavior in $\Gamma(T)$ at low T is different from the classical prediction. Furthermore, in order to determine the origin of the finite Γ at low T, we performed measurements of magnetic correlations on a crystal analyzer spectrometer installed at a pulsed spallation-neutron source, and also on a triple-axis spectrometer at a steady-state neutron source, and it was found that κ is proportional to T,[19] as predicted by classical theory.[11] The finite energy width at low T is thus not caused by a simple relation of $\Gamma(T)$ to $\kappa(T)$ in terms of classical theory, and, it indicates that the $S=3/2$ system exhibits some quantum fluctuations at low temperatures.[18,19]

At present, we have newly performed measurements of magnetic excitations at energy transfers smaller than 20 meV using a chopper spectrometer, to obtain comprehensive data to describe the spin dynamics at low temperatures in $CsVCl_3$. And also, we have performed inelastic-neutron-scattering experiments on $CsVBr_3$ to confirm the dynamical scattering function at low temperatures and the temperature dependence of the energy width of the magnetic excitations, since $CsVBr_3$ is also a good realization of an $S=3/2$ system with $|J'/J|\sim 10^{-4}$ and with $T_N=20.3\,\mathrm{K}$.[21,22,25] Note that the exchange constant was estimated to be $J=90-100\,\mathrm{K}$ from bulk-susceptibility measurements,[25] which is smaller than that in $CsVCl_3$. By comparing the spin dynamics in $CsVCl_3$ with that in $CsVBr_3$, the J dependence of the spin dynamics can be discussed. Using the present result, we reanalyzed the data in our previous experiments, and then presented a comprehensive description of the spin dynamics in $S=3/2$ systems.

II. EXPERIMENTS

We performed inelastic-neutron-scattering experiments to determine the dynamical scattering function $S(q,\omega)$ ($\hbar\omega$ is the energy transfer) describing the spin dynamics in $S=3/2$, 1D Heisenberg antiferromagnets, $CsVCl_3$ and $CsVBr_3$. The scattering function $S(q,\omega)$ in $CsVCl_3$ at a low temperature and its temperature dependence were measured on the chopper spectrometer, MARI,[26] installed at the ISIS Facility (pulsed spallation-neutron source) at the Rutherford Appleton Laboratory. The dispersion relation of the magnetic excitations in $CsVBr_3$ at low temperature was also measured on MARI, and the temperature dependence of the dynamical scattering function was measured on the chopper spectrometer INC,[27] installed at the pulsed spallation-neutron source, KENS, at the High Energy Accelerator Research Organization (KEK). In order to determine the magnetic correlation function in $CsVCl_3$, experiments were performed on the crystal analyzer spectrometer PRISMA[28] at ISIS, and also on the ISSP triple-axis spectrometer PONTA installed at the 5 G beam hole at the JRR-3M reactor at the Tokai establishment of the Japan Atomic Energy Research Institute. In this section, details concerning the experiments are described.

A. Scans on chopper spectrometers

The dynamical scattering function in the present systems was measured on the chopper spectrometers. We first describe the scans on a chopper spectrometer.

A chopper spectrometer is defined as a direct-geometry spectrometer coupled to a pulsed-neutron source. Pulsed polychromatic beams generated at the neutron source are

monochromatized by a mechanical chopper synchronized with the repetition of neutron pulses (50 Hz for ISIS and 20 Hz for KENS), where the chopper is placed between the source and the sample. Neutrons scattered by the sample are detected at a detector system covering a wide range of scattering angles (ϕ) from 3° to 135° on MARI, and from 5° to 130° on INC. In particular, the scattering angles lower than approximately 10° are densely covered by many detectors: the low-angle banks accommodate 140 detectors on MARI ($\phi=3°-10°$) and 30 detectors on INC ($\phi=5°-12°$). The other high-angle detectors are mounted vertically on MARI (12°–135°), and horizontally on INC (17°–130°). The energy transfer and momentum transfer are determined from the time-of-flight (TOF) of the detected neutrons. Since the kinematical factor k_f/k_i (k_i and k_f are the incident and the final neutron wave vectors) which generally appears in the inelastic neutron-scattering cross section is corrected, the observed spectrum can be expressed as $S(q,\omega)$, when adding the other background.

By utilizing the 1D character of the magnetic system, the following advantageous scans are realized. In the scan geometry with the scattering angle ϕ and the crystal angle ψ between k_i and the c^* axis (the direction of these angles are defined against k_i), q is given by

$$q=k_i\cos\psi-k_f\cos(\phi+\psi). \tag{1}$$

In a scan with $\psi=90°$ (i.e., $k_i\perp c^*$), the overall profile of the magnetic excitations can be observed. For the incident neutron energy, $E_i=123$ meV, the scan loci of detectors continuously cover the scattering angles from 3° to 30° on MARI, as indicated in Fig. 1(a) with a sinusoidal dispersion curve having $E_{ZB}=75$ meV. The magnetic intensities can be observed at the crossing points between the dispersion curve and the scan loci. By changing ψ, the covering (q,ω) space is shifted. Holding the relation of $\phi+\psi=90°$, the detector at ϕ realizes a constant-q scan at $q=k_i\cos\psi$ [Fig. 1(b)]. In this scan with ψ near to 90°, each detector scans a different locus from the others. Generally speaking, the counting rate at one detector scanning near to the zone boundary is enough only for determining the peak position, whereas the scattering function can also be determined near to the magnetic zone center due to the intense structure factor using the spectrum from one detector.

In another scan with $\psi=0°$ ($k_i\|c^*$), an important advantage exists for improving the counting rate. Although limited points in the (q,ω) space can be scanned [Fig. 1(a)], this scan geometry enables the integration of all scattering intensities detected at lower scattering angles, since $q=k_i-k_f\cos\phi$ is almost unchanged at low scattering angles. Since 140 detectors and 30 detectors are installed at low scattering angles on MARI and on INC, respectively, a large intensity gain can be realized. In the scan of the measurements on $CsVCl_3$, for instance, the scan locus with $E_i=150$ meV crosses the dispersion curve at three points, and, moreover, just touches near to the zone boundary, and therefore, four points with different q can be scanned at the same time in this scan geometry. Because the angle between the locus and the dispersion curve is different at each peak, due to the resolution effect, the intensity ratio among the peaks is very sensitive to the energy widths. The spectrum observed on this scan can be used for the examination of the scattering function with good statistics.

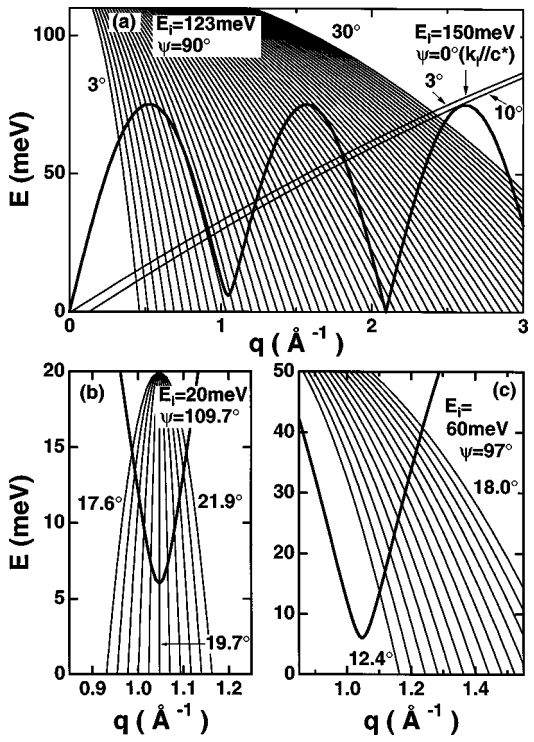

FIG. 1. Scan loci on a chopper spectrometer in measurements of magnetic excitations from $CsVCl_3$ with a dispersion curve (sinusoidal curve) with $E_J=75$ meV and $E_0=0.25$ meV in Eqs. (3) and (4) for different scans. Scans with $E_i=123$ meV and $\psi=90°$ ($k_i\perp c^*$) and with $E_i=150$ meV and $\psi=90°$ ($k_i\|c^*$) are indicated in (a), a scan with $E_i=20$ meV and $\psi=109.7°$ in (b) and a scan with $E_i=60$ meV and $\psi=97°$ in (c), where ψ is the angle between k_i and the c^* axis. The angles indicated near to the loci represent the scattering angles of the corresponding detectors.

B. Measurements of dynamical scattering function in $CsVCl_3$

The dynamical scattering function $S(q,\omega)$ in $CsVCl_3$ at $T=40$ K above T_N was measured on MARI. We previously reported the experiment with $E_i=123$ meV and $\psi=90°$ ($k_i\perp c^*$) in order to observe the overall profile of $S(q,\omega)$.[16] In this experiment, the sample comprised nine single crystals (40 g), of which the c^* axes were tried to be aligned, however, the misalignment of the crystal axes among the sample crystals was relatively large. Therefore, analyzable data were taken only at higher energy transfers where each magnetic excitation could identify its original crystal piece, but the excitations at around the magnetic zone center were not able to be analyzed due to a superimposition of the spectra from misaligned crystals. In this measurement, the spectrum was accumulated for more than 18.5 mA h of proton injection to a tantalum target (18.5 mA h corresponds to 92.5 h at 200 μA of the typical proton current at ISIS). At present, in order to determine $S(q,\omega)$, especially at the zone center, we performed measurements with $E_i=20$ meV and $\psi=109.7°$ and with $E_i=60$ meV and $\psi=97°$, using a sample comprising one single crystal (15 g), with the proton injection of 2.2 and 3.0 mA h, respectively. The mosaic spread was measured to

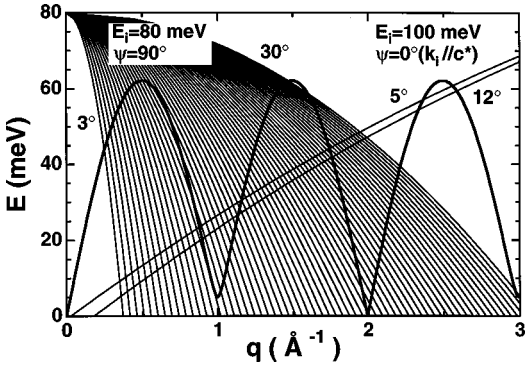

FIG. 2. Scan loci on a chopper spectrometer in measurements of magnetic excitations from $CsVBr_3$ with a dispersion curve (sinusoidal curve) with $E_J=62$ meV and $E_0=0.2$ meV in Eqs. (3) and (4) for different scans. Scans with $E_i=80$ meV and $\psi=90°$ ($k_i \perp c^*$) and with $E_i=100$ meV and $\psi=90°$ ($k_i \| c^*$) are indicated, where ψ is the angle between k_i and the c^* axis. The angles indicated near to the loci represent the scattering angles of the corresponding detectors.

be 2.1° at the full width at half maximum (FWHM). In the scan with $E_i=20$ meV and $\psi=109.7°$, the constant-q scan is realized at the detector with $\phi=19.7°$, as shown in Eq. (1), and excitations with energy transfers up to 15 meV could be measured, and excitations at energy transfers from 15 to 30 meV were measured in the scan with $E_i=60$ meV and $\psi=97°$. The energy resolution was determined to be 2.8, 4.3, and 0.8 meV at FWHM in the scans with $E_i=123$, 60, and 20 meV, respectively, by measuring the energy width of the incoherent elastic scattering. In the scan with $E_i=60$ meV, the slit package with a coarse collimation was used in the mechanical chopper to gain a greater neutron flux. The scan loci for these scans are indicated in Fig. 1.

In order to measure the temperature dependence of $S(q,\omega)$, the experiments on MARI were performed with $E_i=150$ meV and $\psi=0°$ ($k_i \| c^*$) at $T=40$, 50, 80, 120, and 200 K.[15,18] Each spectrum was accumulated for approximately 4 mA h of proton injection. The sample comprised nine single crystals (15 g), of which the c^* axes were accurately aligned. The mosaic spread of the sample, including the misalignment among the single crystals, was measured to be 3.7° at FWHM, and the energy resolution was determined to be 3.6 meV at FWHM by measuring the energy width of the incoherent elastic scattering. The scan loci in this scan are also indicated in Fig. 1.

C. Measurements of dynamical scattering function in $CsVBr_3$

The dispersion relation of magnetic excitations in $CsVBr_3$ (see Fig. 2) at $T=25$ K above T_N was measured on MARI with $E_i=80$ meV and $\psi=90°$ ($k_i \perp c^*$). In this experiment, we used a single-crystal sample weighing 20 g, and, the spectrum was accumulated for more than 5.5 mA h of proton injection, using a chopper with a coarsely collimated slit package in order to gain a greater neutron flux. The energy resolution was determined to be 3.7 meV by measuring the energy width of the incoherent elastic scattering. Due to the large mosaic spread of the crystal, $S(q,\omega)$ was hard to determine, and thus only the dispersion relation was determined in this measurement. $S(q,\omega)$ at around the magnetic

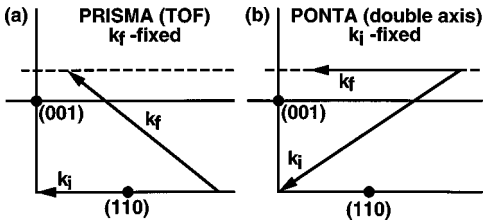

FIG. 3. Scan diagram on the reciprocal plane for measurements of magnetic correlations: (a) on a crystal analyzer spectrometer (PRISMA) and (b) on a triple-axis spectrometer (PONTA) in the double-axis mode. k_i and k_f are the incident and the final wave vectors.

zone center at $T=25$ K was measured on INC in the scan with $E_i=47$ meV and $\psi=102.2°$ by using one single crystal. In this scan, the constant-q scan was performed at the detector with $\phi=12.2°$. The mosaic spread was measured to be 1.6° at FWHM, and the energy resolution was determined to be 2.5 meV by measuring the energy width of the incoherent elastic scattering. The temperature dependence of $S(q,\omega)$ was also measured on INC with $E_i=100$ meV and $\psi=0°$ ($k_i \| c^*$) at $T=25$, 80, 130, and 190 K using a sample comprising four single crystals (40 g). The mosaic spread of the sample, including the misalignment among the single crystals, was measured to be 4.5° at FWHM, and the energy resolution was determined to be 4.8 meV by measuring the energy width of the incoherent elastic scattering. Each spectrum was accumulated for approximately 0.2 mA h of proton injection (0.2 mA h corresponds to 40 h at 5 μA of the typical proton current at KENS).

D. Measurements of magnetic correlations in $CsVCl_3$

In order to determine $\kappa(T)$, the inelastic neutron-scattering experiments were performed on the crystal analyzer spectrometer PRISMA, and also on the ISSP triple-axis spectrometer PONTA.[19]

On PRISMA, the c^* axis ([001]) of a single-crystal sample of $CsVCl_3$ weighing 15 g was mounted perpendicular to k_i and with [110] horizontal, where the constant-q scan at $q=k_f \sin\phi$ is realized for each detector with its scattering angle ϕ, as shown in the scan diagram in Fig. 3. In order to reduce the contamination of higher-order neutron wavelengths, a pyrolytic graphite (PG) filter was placed between the sample and the analyzer crystal. A 60′ collimator was located between the PG filter and the analyzer crystal. The final energy was chosen to be $E_f=12.7$ meV, because the PG filter works efficiently around this energy region and the energy integration up to 100 meV over the zone-boundary energy can be realized. The mosaic spread of the sample crystal was measured to be 2.1° at FWHM, and the q resolution was measured to be $\Delta q=0.02$ Å^{-1} at FWHM by removing the PG filter. In this experimental setup, the inelastic spectrum, $I(q,\omega)$, was taken at each q by moving the analyzer-detector arms step by step (i.e., by changing ϕ). Since $I(q,\omega)$ is the sum of the magnetic scattering cross section $(k_f/k_i)S(q,\omega)$ and the other background, the correlation function $S(q)$ was deduced by integrating $(k_i/k_f)I(q,\omega)$ over $\hbar\omega$ up to 100 meV.

A conventional double-axis measurement was also performed. The triple-axis spectrometer PONTA was operated

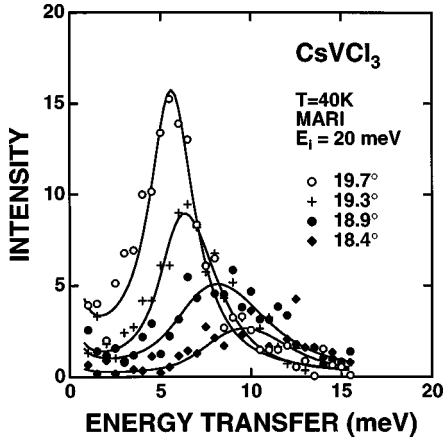

FIG. 4. Inelastic spectra of $CsVCl_3$ at $T=40$ K at around the magnetic zone center measured in the scan with $E_i=20$ meV and $\psi=109.7°$ shown in Fig. 1(b). The solid lines are the fitted curve by a Lorentzian scattering function (see text). The scan at the detector with $\phi=19.7°$ is the constant-q scan at the magnetic zone center.

in the double-axis mode with the incident neutron energy E_i fixed at 30.5 meV using the collimation 15′-20′-20′. A single-crystal sample of $CsVCl_3$ weighing 1 g was mounted with [110] and [001] in the scattering plane. The scan was performed keeping the 1D reciprocal lattice plane parallel to k_f in order to realize the geometrical condition of the energy integration at each q (Fig. 3). The mosaic spread of the sample crystal was measured to be 0.9° at FWHM, and the resolution was measured to be $\Delta q=0.02$ Å^{-1} at FWHM by removing the PG filter.

III. RESULTS

A. $S(q,\omega)$ at low temperatures

Figure 4 shows the inelastic spectra from $CsVCl_3$ at around the magnetic zone center at $T=40$ K in the scan with $E_i=20$ meV and $\psi=109.71°$. At the detector with $\phi=19.7°$, the constant-q scan was realized at the magnetic zone center. The observed spectra for individual detectors in the scans with $E_i=20$ meV and $\psi=109.7°$, $E_i=60$ meV and $\psi=97°$ and $E_i=123$ meV and $\psi=90°$ were fitted to the following scattering function convoluted with the instrumental resolution:

$$S(q,\omega)=[n(\omega)+1]F(Q)^2A(q)\frac{\Gamma(q)/\pi}{[\hbar\omega-E(q)]^2+\Gamma(q)^2}, \tag{2}$$

where $[n(\omega)+1]$ is the thermal population factor $[\exp(-\hbar\omega/k_BT)-1]^{-1}$, and Q is the scattering vector. The magnetic form factor $F(Q)$ was taken from the calculated value of the V^{2+} free ion.[29] The resolution function[30] was calculated using a Gaussian approximation based on the neutron pulse width, the chopper burst time width and the geometrical configuration of the spectrometer in the same manner as the Cooper-Nathans resolution matrix;[31] also, the effect of the sample mosaic spread was also properly included.[32] The resolution correction for the inelastic neutron-scattering experiment at the pulsed neutron sources presently reaches the level of the well-established resolution

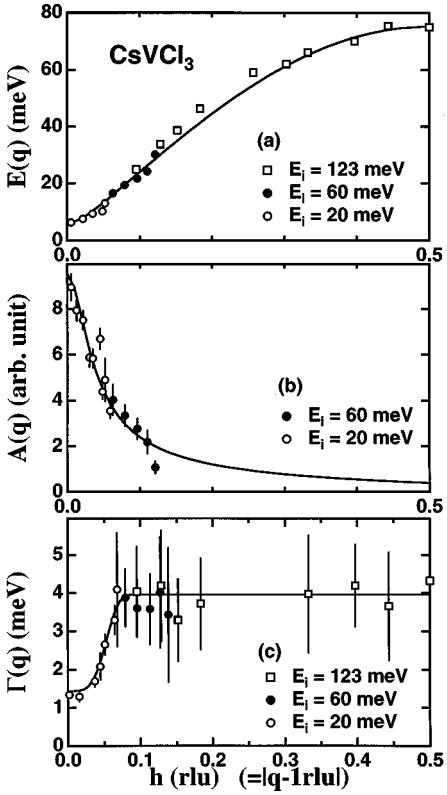

FIG. 5. The q dependence of the energy $E(q)$, the structure factor $A(q)$, and the energy width $\Gamma(q)$ of the magnetic excitations from $CsVCl_3$, are plotted against the wave number from the magnetic zone center ($h=|q-1$ rlu$|$) in (a), (b), and (c). The energy positions (squares) in (a) are taken from Refs. 15 and 17. The solid line in (a) is the fitted curve with Eqs. (3) and (4), and that in (b) is the calculated curve with Eqs. (3) and (5) from the obtained parameters in $E(q)$. By the fit, $E_J=75$ meV and $E_0=0.24$ meV in Eq. (3) were obtained. The solid line in (c) is a guide to the eye.

correction for inelastic measurements using the triple-axis method. The observed energy resolution for any scan in the present report mentioned above was in very good agreement with the calculation. In the fit, the peak energy $[E(q)]$, the structure factor $[A(q)]$ and the energy width $[\Gamma(q)]$ of the magnetic excitation were parametrizing on the assumption that these parameters are constants independent of q in each spectrum. As shown in Fig. 4, the fit was successful, and Fig. 5 shows $E(q)$, $A(q)$, and $\Gamma(q)$ obtained by the fit. In Fig. 5, $E(q)$, $A(q)$, and $\Gamma(q)$ are plotted against the wave number from the magnetic zone center ($h=|q-1$ rlu$|$) in units of reciprocal-lattice unit (rlu, 1 rlu$=1.05$ Å^{-1} at $T=40$ K). The normalization in $A(q)$ between the scans was made by using the intensity of the data at q overlapped between the scans. As shown in Fig. 5(a), the obtained dispersion relation $E(q)$ was well fitted to the following equations:

$$E(q)=\sqrt{u(q)v(q)} \tag{3}$$

with

$$u(q)=E_J(1-\cos aq),$$

$$v(q)=E_J(1+\cos aq)+E_0, \tag{4}$$

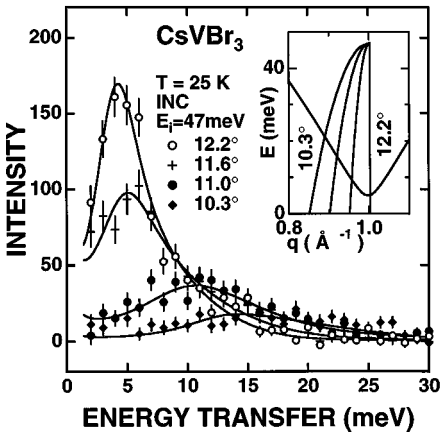

FIG. 6. Inelastic spectra of $CsVBr_3$ at $T=25$ K at around the magnetic zone center measured in the scan with $E_i=47$ meV and $\psi=102.2°$. The solid lines are the fitted curve by a Lorentzian scattering function (see text). The scan at the detector with $\phi=12.2°$ is the constant-q scan at the magnetic zone center. The inset shows the scan loci for the four detectors corresponding to the spectra.

where a is the lattice constant, and E_J and E_0 were obtained to be 75.0 ± 0.7 meV and 0.24 ± 0.02 meV, respectively. Assuming $E_J=4SRJ$ with the renormalization constant (R) calculated from the quantum Monte Carlo method,[33] the exchange constant was determined to be $J=119\pm3$ K. The excitation energy at the magnetic zone center was measured to be 6.0 ± 0.2 meV. The structure factor can be calculated from $u(q)$ and $v(q)$ as follows:

$$A(q)=\sqrt{u(q)/v(q)}. \tag{5}$$

The solid line in Fig. 5(b) is the structure factor $A(q)$ calculated by Eq. (5) with the parameters obtained by the fit of $E(q)$. The observed structure factor was in good agreement with that described by Eq. (5). Figure 5(c) shows $\Gamma(q)$ obtained by the fit, $\Gamma(q)$ was constant at larger energy transfers corresponding to $h>0.07$ rlu as we reported previously, however, at present, we newly found $\Gamma(q)$ exhibits the minimum of 1.3 ± 0.3 meV at the magnetic zone center. $S(q,\omega)$ in $CsVCl_3$ determined at present well describes the inelastic spectrum in the scan with $E_i=150$ meV and $\psi=0°$ ($k_i\|c^*$), as shown in Fig. 8, and Γ at the constant region was obtained to be 3.2 ± 0.4 meV by fitting the spectrum in this scan (details of the fit are described in the following section).

Figure 6 shows the inelastic spectrum from $CsVBr_3$ at around the magnetic zone center at $T=25$ K above T_N in the scan with $E_i=47$ meV and $\psi=102.2°$ measured on INC. In this scan, the constant-q scan was performed at the magnetic zone center at the detector with $\phi=12.2°$. The observed spectra for individual detectors were fitted to $S(q,\omega)$ in Eq. (2) convoluted with the instrumental resolution, in the same manner as the analysis of the $CsVCl_3$ data, and in Fig. 7, $E(q)$, $A(q)$, and $\Gamma(q)$ obtained by the fit are plotted against the wave number from the zone center (h). In Fig. 6(a), the positions of the magnetic excitations from $CsVBr_3$ observed at $T=25$ K in the scan with $E_i=80$ meV and $\psi=0°$ on MARI are also plotted. The positions of the excitations $E(q)$ were well fitted to the dispersion relation describing by Eqs. (3) and (4), and E_J and E_0 were obtained to be 62.0

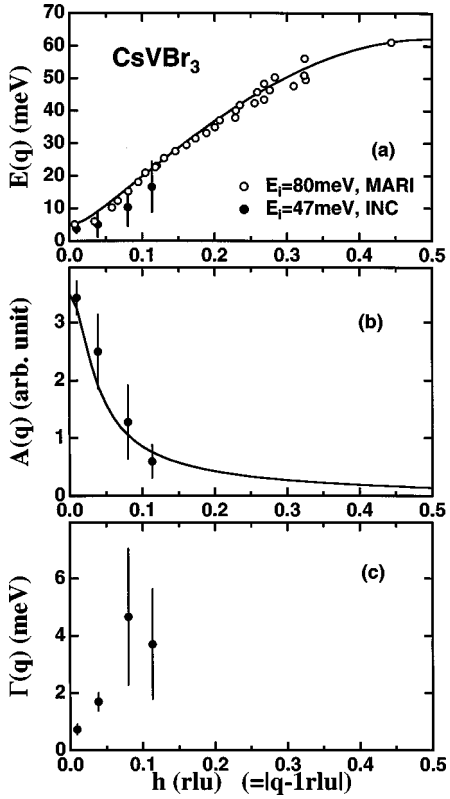

FIG. 7. The q dependence of the energy $E(q)$, the structure factor $A(q)$, and the energy width $\Gamma(q)$ of the magnetic excitations from $CsVBr_3$, are plotted against the wave number from the magnetic zone center ($h=|q-1$ rlu$|$) in (a), (b), and (c). The solid line in (a) is the fitted curve with Eqs. (3) and (4), and that in (b) is the calculated curve with Eqs. (3) and (5) from the obtained parameters in $E(q)$. By the fit, $E_J=62$ meV and $E_0=0.2$ meV in Eq. (3) were obtained.

±0.5 meV and 0.20 ± 0.02 meV, respectively, by the fit. Assuming $E_J=4SRJ$ again, J was determined to be 99 ± 3 K. The zone-center energy was measured to be 5.0 ± 0.2 meV. The structure factor $A(q)$ can be calculated from the obtained parameters describing $E(q)$, and the observed $A(q)$ was in good agreement with the calculation, as shown in Fig. 7(c). We found that $\Gamma(q)$ in $CsVBr_3$ at $T=25$ K also exhibits the minimum of 0.7 ± 0.2 meV at the magnetic zone center. $S(q,\omega)$ in $CsVBr_3$ determined at present well describes the inelastic spectrum in the scan with $E_i=100$ meV and $\psi=0°$ ($k_i\|c^*$) measured on INC, as shows in Fig. 9, and based on the assumption of Γ being independent of q at larger energy transfers, Γ at the constant region was obtained to be 2.4 ± 0.3 meV by fitting the spectrum (details of the fit are described in the following section).

The obtained parameters describing the energy scale in $S(q,\omega)$ at low temperatures are summarized in Table I. E_J in Eq. (3), which is approximately the zone-boundary energy, was obtained from fitting the dispersion relation, the zone-center energy ($E_{ZC}=\sqrt{2E_JE_0}$) and the zone-center energy width (Γ_{ZC}) were from fitting the inelastic spectra in the constant-q scans at the magnetic zone center, and the q-independent energy width at larger energy transfer (Γ) was obtained from fitting the inelastic spectra in the scan with $k_i\|c^*$. We found that all of the parameters describing the energy scale can be scaled by the exchange constants.

TABLE I. Parameters describing the energy scale in $S(q,\omega)$ in $CsVCl_3$ and $CsVBr_3$ at low temperatures ($T=40$ and 25 K, respectively): E_J in Eq. (4), the zone-center energy E_{ZC}, the zone-center energy width Γ_{ZC}, and the energy width at the q-independence region at larger energy transfers Γ. The exchange constant (J) was determined from $E_J=4SJR$ with the renormalization factor (R) from the quantum Monte Carlo calculation. The experimental errors were estimated from the statistical errors of neutron counts and the accuracy of R.

Parameters	$CsVCl_3$	$CsVBr_3$
E_J (meV)	75.0±0.7	62.0±0.5
E_{ZC} (meV)	6.0±0.2	5.0±0.2
Γ_{ZC} (meV)	1.3±0.3	0.7±0.2
Γ (meV)	3.2±0.4	2.4±0.3
J (meV)	10.3±0.3 (119 K±3 K)	8.5±0.2 (99 K±3 K)
E_{ZC}/J	0.58±0.03	0.59±0.03
Γ_{ZC}/J	0.13±0.03	0.08±0.02
Γ/J	0.31±0.04	0.28±0.04

B. Temperature dependence of energy widths

Figure 8 shows the inelastic spectra from $CsVCl_3$ in the scan with $E_i=150$ meV and $\psi=0°$ ($k_i \| c^*$). Each inelastic spectrum was well fitted to the following scattering function adding background:

$$I(q,\omega)=c_1 S(q,\omega)+c_2+c_3\exp(-c_4\hbar\omega)+c_5\exp[-(\hbar\omega-c_6)^2/c_7^2]. \quad (6)$$

The magnetic dynamical scattering function $S(q,\omega)$ is described by Eq. (2) convoluted with the above-mentioned instrumental resolution function. The other terms in Eq. (6) represent the background with adjustable parameters c_i ($i=1-7$). The Gaussian term in Eq. (6) represents a phonon background from the sample itself. The background measurements performed at detectors located off the scattering plane by turning the crystal by 90° showed a peak at around $\hbar\omega=21$ meV, of which origin is supposed to be phonons from the crystal itself. The inelastic spectrum observed in the background measurements can be fitted to the background terms in Eq. (6). The fit of the present inelastic spectra in the scan with $E_i=150$ meV and $\psi=0°$ gave the parameters describing the background [c_i ($i=2-7$)] not identical to those in the fit of the background spectrum, but close to those. In order to express the background better, the parameters describing the background were parametrized. Although this background correction is different from that in our previous report,[15–18] and the presently obtained parameters describing $S(q,\omega)$ were slightly different from the previous values, they were qualitatively the same results as those in the previous report. This correction can express the functional form of the background better than the previous analysis, and from the present background correction, a consistent result could be obtained for the parameters describing $S(q,\omega)$ and in the description of the two compounds $CsVCl_3$ and $CsVBr_3$, as described below. It is noted that the obtained parameters, c_i ($i=1-7$), were almost independent of T, except that the width of phonons c_7 was broadened with increasing T. The present background correction improved our data analysis.

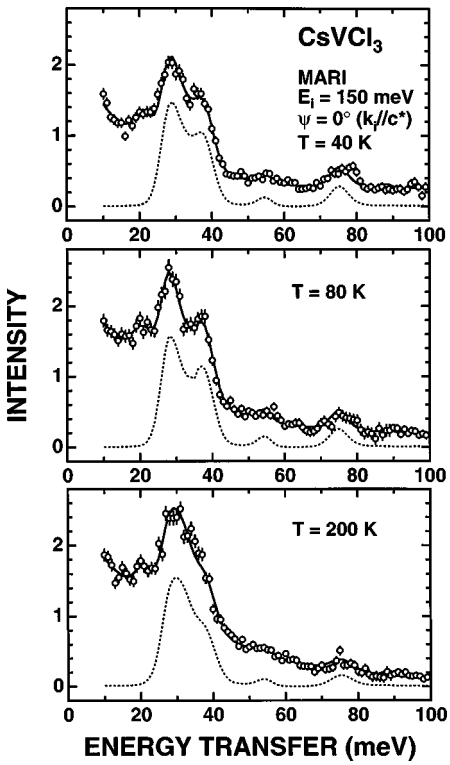

FIG. 8. The temperature dependence of the inelastic spectra of $CsVCl_3$ measured on MARI in the scan with $E_i=150$ meV and $\psi=90°$ ($k_i \| c^*$) indicated in Fig. 1(a). The solid lines are the fitted curves with the sum of a Lorentzian scattering function convoluted with the instrumental resolution and a background (see text). The dashed lines are the dynamical magnetic scattering function obtained by the fit.

First, we tried to fit the data at $T=40$ K with Eq. (6) using the above-determined functional forms with $E(q)$, $A(q)$, and $\Gamma(q)$ [adjustable parameters are c_i ($i=1-7$) only], and found good agreement. Second, we tried to fit the same data by parametrizing the value of Γ at the q-independent region ($h>0.07$ rlu) while holding the minimum energy width at the zone center to be the observed value. The result of the fit was identical to that in the first trial, and Γ at the q-independent region was obtained to be 3.2 meV, which agreed with $\Gamma(q)$ shown in Fig. 5(c) within the experimental errors. Third, we tried to fit the same data on the assumption of $E_0=0$ meV and q-independent Γ at any q. As shown in Fig. 8, it was well fitted to the data, and this result of the fit was also identical to those in the first and second trials, and Γ was obtained to be 3.2 ± 0.4 meV. The magnetic excitations in the scan with $E_i=150$ meV and $\psi=0°$ were observed at energy transfers greater than 20 meV, and $\Gamma(q)$ in Fig. 5(c) is shown to be independent of q in the q-range corresponding to the energy transfers. Moreover, $\Gamma(q)$ near to the magnetic zone center is smaller, as shown in Fig. 5(c), eventually, the above-mentioned three trials for the fits gave the identical result and is consistent with our previous report.

In the analysis of the temperature dependence of the spin dynamics in $CsVCl_3$, the observed inelastic spectra in the scan taken on MARI with $E_i=150$ meV and $\psi=0°$ were fitted to Eq. (6) on the assumption of $E_0=0$ meV and q-independent Γ at any q. The fit was very successful at any

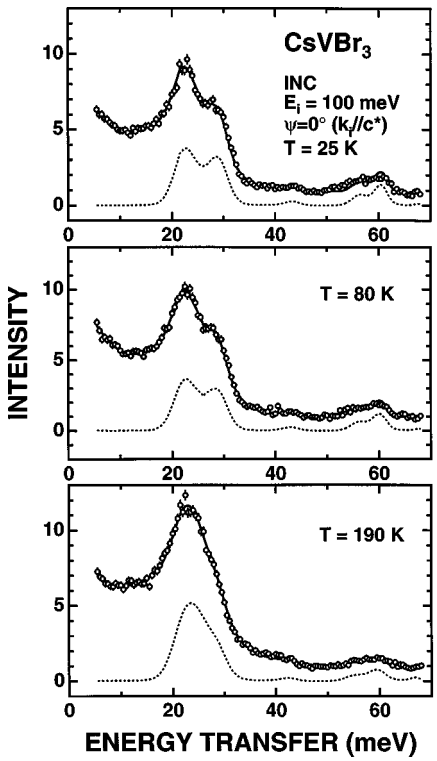

FIG. 9. The temperature dependence of the inelastic spectra of $CsVBr_3$ measured on INC in the scan with $E_i=150$ meV and $\psi=90°$ ($k_i \| c^*$) indicated in Fig. 2. The solid lines are the fitted curves with the sum of a Lorentzian scattering function convoluted with the instrumental resolution and a background (see text). The dashed lines are the dynamical magnetic scattering function obtained by the fit.

T, as shown in Fig. 8. Figures 10 and 11 show the obtained T dependence of $\Gamma(T)$ and the sum, $\Gamma(T)+E_J(T)$, respectively. For $CsVBr_3$, the observed inelastic spectra in the scan taken on INC with $E_i=100$ meV and $\psi=0°$ were fitted to Eq. (6) on the same assumption as that for $CsVCl_3$. The fit for $CsVBr_3$ was also very successful at any T, as shown in Fig. 9. The obtained $\Gamma(T)$ and the sum, $\Gamma(T)+E_J(T)$, are also plotted in Figs. 10 and 11, respectively. In the plot shown in Figs. 10 and 11, the abscissas and ordinates were normalized by the exchange constants J determined from the dispersion relations at low temperatures. We found the following properties in the energy widths of the magnetic excitations: $\Gamma(T)$ can be scaled by J, at temperatures $T>J$, $\Gamma(T)$ is proportional to T as predicted by classical theory,[10] and at $T<J$, Γ decreases with decreasing T and becomes finite at low temperatures. The ratio of the sum $\Gamma(T)+E_J(T)$ to J was also found to be independent of T within the experimental errors.

C. Temperature dependence of magnetic correlations

Figure 12 shows the q dependence of the energy-integrated spectrum in $CsVCl_3$ taken on PRISMA, where the kinematical factor k_f/k_i was corrected and the upper limit of the energy integration was 100 meV over the zone-boundary energy of the dispersion relation of the magnetic excitations in $CsVCl_3$. The q-dependent spectra at each T was well fitted to the sum of the Lorentzian scattering function $[\sim(q^2+\kappa^2)^{-1}]$ convoluted with the Gaussian q resolution and a sloping background in q, as shown in Fig. 12, and $\kappa(T)$ was obtained as shown in Fig. 14. Figure 13 shows the q-dependent energy-integrated spectrum measured in the double-axis mode on PONTA. The q dependence of the observed intensity was also well fitted with the sum of the Lorentzian scattering function $[\sim(q^2+\kappa^2)^{-1}]$ convoluted with the Gaussian q resolution and a sloping background, as shown in Fig. 13. $\kappa(T)$ obtained from this experiment is also plotted in Fig. 14.

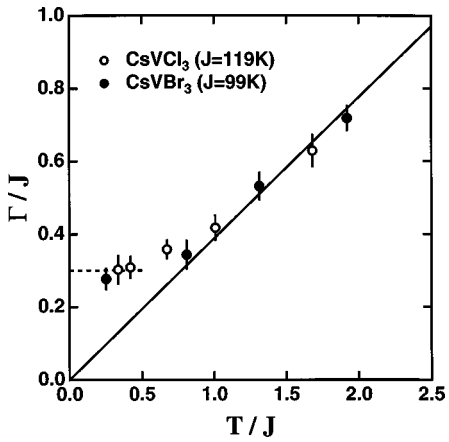

FIG. 10. The temperature dependence of the energy width (Γ) of the magnetic excitations from $CsVCl_3$ and $CsVBr_3$. The abscissa and ordinate were normalized by the exchange constants (J) determined from the dispersion relations at low temperatures. We found that Γ/J is proportional to T/J at high temperatures $T/J>1$ and becomes finite at low temperatures. The dashed line is the guide to the eye.

From these two measurements, different results concerning $\kappa(T)$ were obtained, as shown in Fig. 14. The magnetic correlation function is defined by the magnetic response $S(q,\omega)$ integrated over $\hbar\omega$, and the inelastic neutron-scattering cross section is proportional to $S(q,\omega)$ multiplied by the kinematical factor k_f/k_i. This quantity was measured in the PRISMA experiment with the integration covering all

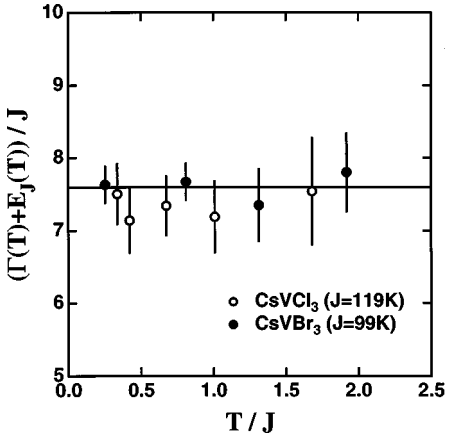

FIG. 11. The temperature dependence of the sum $\Gamma+E_J$ [E_J is the parameter in Eq. (3)] from $CsVCl_3$ and $CsVBr_3$. Abscissa and ordinate were normalized by the exchange constants (J) determined from the dispersion relations at low temperatures. We found that $(\Gamma+E_J)/J$ is independent of T/J at any temperatures.

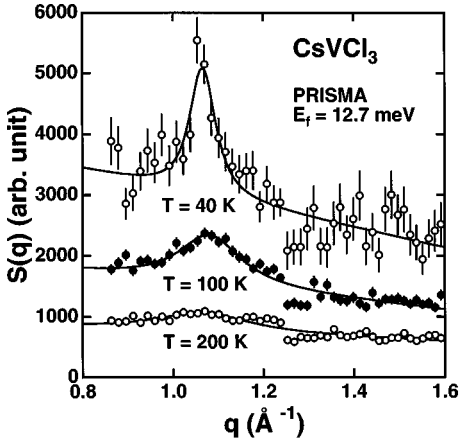

FIG. 12. The temperature dependence of the q-dependent energy-integrated spectra from $CsVCl_3$ measured on PRISMA, where the kinematical factor k_f/k_i was corrected. The solid lines are the fitted curves with the sum of a Lorentzian correlation function convoluted with the instrumental resolution and a sloping background.

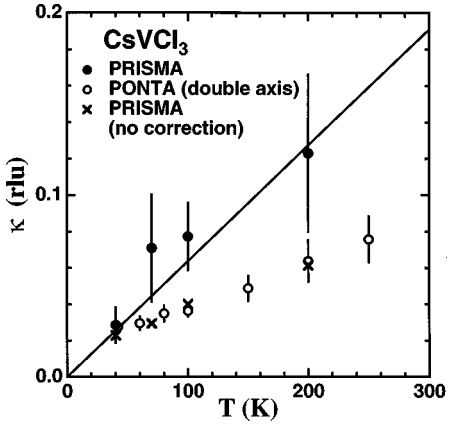

FIG. 14. The temperature dependence of the inverse magnetic correlation length $\kappa(T)$ in $CsVCl_3$ taken on PRISMA (closed circles), on PONTA in the double-axis mode (open circles), and deduced from the PRISMA data without correcting k_f/k_i (crosses). The solid line is the classical prediction for $J=119$ K.

excitation energies up to the zone boundary. On the other hand, the energy-integrated spectrum obtained from the conventional double-axis measurement is the integration of the cross section without correcting the kinematical factor, however, the integration range is bounded by the upper limit E_i, much lower than the zone-boundary energy. Therefore, the PRISMA results present a more accurate probe of the magnetic correlations. In fact, the energy-integrated spectrum from $I(q,\omega)$ taken on PRISMA without correcting k_f/k_i was also well fitted to the Lorentzian scattering function with a background, and $\kappa(T)$ obtained by the fit was identical to the result from the double-axis measurement, as shown in Fig. 14. The difference shown in Fig. 14 thus mainly comes from the correction of k_f/k_i. The large error bar of $\kappa(T)$ taken on PRISMA in Fig. 14 comes from an enhancement of the poor statistics of the inelastic spectrum at a larger energy transfer due to the correction of k_f/k_i. The background of the q-dependent spectra taken on PRISMA was dependent on T due to nonmagnetic inelastic scattering enhanced by the kinematical-factor correction, on the other hand, that on PONTA was almost T independent due to the enhancement of the incoherent elastic scattering without any correction. It is noted that, in the point of the experimental technique, the correction of the kinematical factor (k_f/k_i) in the inelastic neutron-scattering cross section is important for the determination of the accurate correlation function in a system having excitations with larger transfer energy relative to the incident neutron energy.

In classical theory, $\kappa(T)$ is expressed by $\kappa(T)=T/(2JS^2a)$ at low temperatures, where J is the exchange constant and a is the lattice constant.[11] The solid line in Fig. 14 is $\kappa(T)$, calculated from this formula, with $J=119$ K determined from the dispersion relation described above.

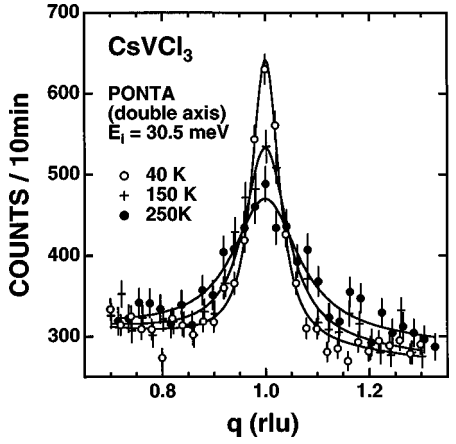

FIG. 13. The temperature dependence of the q-dependent energy-integrated spectra from $CsVCl_3$ measured on PONTA in the double-axis mode. The solid lines are the fitted curves with the sum of a Lorentzian correlation function convoluted with the instrumental resolution and a sloping background.

IV. DISCUSSIONS

We now discuss the spin dynamics in $S=3/2$, 1D Heisenberg antiferromagnetic systems, $CsVCl_3$ and $CsVBr_3$, on the basis of our inelastic neutron-scattering data taken at the temperatures higher than the 3D ordering temperature T_N. The 1D nature should be discussed at T above T_N, where the effects of the 3D ordered state are negligible.

The form of the dispersion relation in Eqs. (3) and (4) can be deduced from the spin-wave dispersion relation with the intrachain exchange constant (J), the interchain exchange constant (J') and the single-ion anisotropy (D) in the 3D ordered state[23] with the limit of $J'=0$. The dispersion relation of the magnetic excitations in the present systems at low temperatures was well fitted to the dispersion relation in Eqs. (3) and (4). Assuming $E_J=4SRJ$ with the renormalization constant (R) calculated from the quantum Monte Carlo method,[33] the exchange constant was determined to be $J=119\pm3$ K for $CsVCl_3$ and 99 ± 3 K for $CsVBr_3$, which agreed well with that from bulk-susceptibility measurements.[16,25] The obtained finite E_0 causes the finite zone-center energy of 6.0 ± 0.2 meV and 5.0 ± 0.2 meV, for $CsVCl_3$ and $CsVBr_3$, respectively. In the interpretation of the dispersion relation in the 3D ordered state, E_0 should represent D.[23] However, the presently obtained E_0 does not cor-

respond to D, because the parameters (J, J', and D) in the Hamiltonian describing the spin-wave excitations in the 3D ordered state were reported to be determined from the spin-wave excitations from $CsVCl_3$ at $T=1.6$ K much below T_N. At the magnetic zone center, the excitation having much lower energy than the presently observed finite energy was used for the determination, and the spin-wave excitations of the 3D origin were reported to disappear at temperatures near to and above T_N.[24] From the present determination of the $S(q,\omega)$ at low temperatures, we found that all of the parameters describing the energy scale in $S(q,\omega)$ at low temperatures can be scaled by the intrachain exchange constant (J) within the experimental errors, as listed in Table I. This suggests that $S(q,\omega)$ can be described by J only, and it is therefore indicated that the observed spin dynamics is caused by the one dimensionality of the present systems. A recent numerical calculation for an $S=3/2$ system at low temperatures has predicted an excitation continuum with an energy spread up to the energy transfers of $\sim J$ at the magnetic zone center.[34] We observed that the magnetic excitations spread up to the energies of around 10 meV ($\sim J$) at the magnetic zone center, as shown in Figs. 4 and 6. The observed energy spread corresponds to that of the numerically predicted excitation continuum. The numerical calculation has also shown the gapless strong excitation at the magnetic zone center, which is a single spin-wave mode observable only at $T=0$ K. In the present experiments at the finite temperatures, the single spin-wave mode was not observed at the zone center. The lower boundary of the energy spread of the excitation continuum should be $\hbar\omega=0$ meV, and therefore the present result does not contradict the dynamical property predicted by current theory: half-integer spin systems exhibit gapless excitation,[6] and the finite E_0 does not mean the energy gap. It is natural that the observed finite energy width [Γ(half width)$\sim 0.3J$] at larger energy transfers should be interpreted as being the excitation continuum extending from the zone center, since the observed energy spread is on the same order as the predicted continuum spread at the zone center. In order to elucidate especially the origin of the finite zone-center energy and the minimum in $\Gamma(q)$ observed at present, further development of theories describing the present systems is desired.

The measured temperature dependence of the inverse magnetic correlation length (taken on PRISMA) is in good agreement with classical theory, $\kappa(T)=T/(2JS^2a)$,[11] as shown in Fig. 14, and, $\kappa(T)$ can be extrapolated to vanish at $T=0$ K. This result is consistent with current theory at $T=0$ K: half-integer spin systems show power-law decay in the spin correlation and integer spin systems show exponentially decaying correlations.[6] Correlations with power-law decay represent a sort of a long-range ordering, and therefore, $\kappa=0$ at $T=0$ K in terms of κ.[12] The presently obtained linear T dependence of κ at the observed T range is also consistent with the result from the numerical study for an $S=3/2$ system.[12]

Concerning the temperature dependence of the spin dynamics, we found the following properties in the energy widths of the magnetic excitations (Fig. 10): $\Gamma(T)$ can be scaled by J, at temperatures $T>J$, $\Gamma(T)$ is proportional to T, as predicted by classical theory, and at $T<J$, Γ decreases with decreasing T and becomes finite at low temperatures. The scaling by J suggests that the observed spin dynamics is of a 1D origin, again. On the other hand, we found that $\kappa(T)$ is proportional to T at any T. A classical system exhibits ordering at $T=0$ K, and dynamical scaling can be applied to the phase transition. The linear relation between Γ and κ as well as the q-independent Γ is consistent with the scaling. At high temperatures $T>J$, we can conclude the linear relation between $\Gamma(T)$ and $\kappa(T)$ with their linear T dependence. We also found that the sum $\Gamma(T)+E_J(T)$ is independent of T, as shown in Fig. 11. Classical theory has predicted the T dependence of Γ and E_J through $\kappa(T)$ at low T as follows: $\Gamma(T)=2SJ\kappa(T)a$ and $E_J(T)=4SJ[1-\kappa(T)a/2]$.[10] Thus, the sum of the two quantities should be independent of T due to the cancellation of $\kappa(T)$. The present result at $T>J$ in Fig. 11 also shows the validity of the relation (it is noted that the constant sum relation is shown even at $T<J$). Moreover, assuming the q-independent Γ in the analysis, the fit to the observed inelastic spectrum was very successful. Although a direct measurement of $\Gamma(q)$ at around the magnetic zone center is necessary for thoroughly understanding the behavior at high temperatures, we conclude that the spin dynamics at high temperatures $T>J$, is well described by classical theory for a 1D Heisenberg antiferromagnetic system. However, at low temperatures $T<J$, there is no linear relation between $\Gamma(T)$ and $\kappa(T)$. The observed finite energy widths at low T are not $\Gamma(T)$ constructing the scaling with $\kappa(T)$ in terms of classical theory, and the finite width indicates some fluctuations surviving even at low T. A possible reason for the finite energy width is the existence of an excitation continuum, as mentioned above. Therefore, we observed the crossover from the quantum state at low T to the classical state at high T in the $S=3/2$ systems.

V. CONCLUSIONS

We demonstrated the spin dynamics in $S=3/2$, 1D Heisenberg antiferromagnets, $CsVCl_3$ and $CsVBr_3$, using inelastic neutron scattering. Measurements of the dynamical scattering function $S(q,\omega)$ were performed on the chopper spectrometers installed at the pulsed spallation neutron source, and the magnetic correlations were measured on the crystal analyzer spectrometer at the pulsed spallation neutron source as well as on the triple-axis spectrometer with the double-axis mode at the steady-state neutron source. The experiments were performed at temperatures above the 3D ordering temperature T_N in order to discuss the 1D properties in the present systems. We, first, described the dynamical scattering function at low temperatures. The dispersion relation of the magnetic excitations at low temperatures was well fitted to that of an antiferromagnet with an finite zone-center energy. From the obtained parameter describing the dispersion relation, using the renormalization constant obtained from the quantum Monte Carlo method, the exchange constant was determined to be 119 ± 3 K and 99 ± 3 K for $CsVCl_3$ and $CsVBr_3$, respectively, and these values agreed well with those taken in bulk-susceptibility measurements. The observed structure factor was well described by that calculated from the parameters describing the dispersion relation. The energy widths Γ were independent of q at large energy transfers, however, $\Gamma(q)$ exhibits the minimum at the magnetic zone center. The parameters describing the energy

scale in $S(q,\omega)$ at low temperatures, i.e., the zone-boundary energy, the zone-center energy, the energy width at the constant region, and the energy width at the magnetic zone center, were found to be scaled by the exchange constant (J). This suggests that the observed spin dynamics is caused by the one-dimensionality of the present systems. The energy spread of the magnetic excitations at the zone center as well as the finite energy widths at the larger energy transfer suggest the existence of the excitation continuum. We also investigated the temperature dependence of the spin dynamics, and found the following properties in the energy widths (Γ) of the magnetic excitations: $\Gamma(T)$ can be scaled by J, at temperatures $T>J$, $\Gamma(T)$ is proportional to T, as predicted by classical theory, and at $T<J$, Γ decreases with decreasing T and becomes finite at low temperatures. On the other hand, we found that $\kappa(T)$ is proportional to T at any T, as predicted by classical theory as well as recent numerical calculations for an $S=3/2$ system. The scaling by J suggests that the observed spin dynamics is of a 1D origin, again. We conclude that the spin dynamics at high temperatures $T>J$, is well described by classical theory. However, at low temperatures $T<J$, the observed finite energy widths at low temperatures are not $\Gamma(T)$ constructing the scaling with $\kappa(T)$ in terms of classical theory, and, the finite width indicates some quantum fluctuations. Therefore, we demonstrated the crossover from the quantum state at low temperatures to the classical state at high temperatures in $S=3/2$ systems.

ACKNOWLEDGMENTS

This work was performed under the UK-Japan Collaboration Program on Neutron Scattering and a Grant-in-Aid for Scientific Research. Both were supported by the Japanese Ministry of Education, Science, Sports and Culture.

[1] H. A. Bethe, Z. Phys. **71**, 205 (1931).
[2] J. des Cloizeaux and J. J. Pearson, Phys. Rev. **128**, 2131 (1962).
[3] G. Müller, H. Thomas, H. Beck, and J. Bonner, Phys. Rev. B **24**, 1429 (1981).
[4] Y. Endoh, G. Shirane, R. J. Birgeneau, P. M. Richards, and S. L. Holt, Phys. Rev. Lett. **32**, 170 (1974).
[5] S. E. Nagler, D. A. Tennant, R. A. Cowley, T. G. Perring, and S. K. Satija, Phys. Rev. B **44**, 12 361 (1991).
[6] F. D. M. Haldane, Phys. Lett. **93A**, 464 (1983); Phys. Rev. Lett. **50**, 1153 (1983).
[7] M. T. Hutchings, G. Shirane, R. J. Birgeneau, and S. L. Holt, Phys. Rev. B **5**, 1999 (1972).
[8] P. Heller and M. Blume, Phys. Rev. Lett. **39**, 962 (1977).
[9] B. I. Halperin and P. C. Hohenberg, Phys. Rev. **177**, 952 (1969).
[10] G. Reiter and A. Sjölander, Phys. Rev. Lett. **39**, 1047 (1977); J. Phys. C **13**, 3027 (1980).
[11] M. E. Fisher, Am. J. Phys. **32**, 343 (1964).
[12] N. Hatano and M. Suzuki, J. Phys. Soc. Jpn. **62**, 1346 (1993).
[13] S. Yamamoto, Phys. Rev. B **53**, 3364 (1996).
[14] S. Itoh, H. Tanaka, and T. Otomo, J. Phys. Soc. Jpn. **66**, 455 (1997).
[15] S. Itoh, K. Kakurai, M. Arai, and Y. Endoh, J. Phys.: Condens. Matter **5**, 6767 (1993).
[16] S. Itoh, Y. Endoh, K. Kakurai, and H. Tanaka, Phys. Rev. Lett. **74**, 2375 (1995).
[17] S. Itoh, Y. Endoh, K. Kakurai, and H. Tanaka, Physica B **213&214**, 161 (1995).
[18] S. Itoh, Y. Endoh, K. Kakurai, H. Tanaka, and T. G. Perring, Physica B **241-243**, 546 (1998).
[19] S. Itoh, K. Kakurai, Y. Endoh, H. Tanaka, M. J. Harris, and K. Nakajima, J. Phys. Chem. Solids (to be published).
[20] H. Kadowaki, K. Hirakawa, and K. Ubukoshi, J. Phys. Soc. Jpn. **52**, 1799 (1983).
[21] M. Niel, C. Cros, G. le Flem, M. Pouchard, and P. Hagenmuller, Physica B **86-88**, 702 (1977).
[22] R. Feile, J. K. Kjems, A. Hauser, H. U. Güdel, U. Falk, and A. Furrer, Solid State Commun. **50**, 435 (1984).
[23] H. Kadowaki, K. Ubukoshi, K. Hirakawa, D. P. Belanger, H. Yoshizawa, and G. Shirane, J. Phys. Soc. Jpn. **55**, 284 (1986).
[24] T. Inami, K. Kakurai, and H. Tanaka, J. Phys.: Condens. Matter **9**, 1357 (1997).
[25] H. Tanaka, H. Nakano, and S. Matsuo, J. Phys. Soc. Jpn. **63**, 3169 (1994).
[26] A. D. Taylor, M. Arai, S. M. Bennington, Z. A. Bowden, R. Osborn, K. Andersen, W. G. Stirling, T. Nakane, K. Yamada, and D. Welz (unpublished).
[27] M. Arai, M. Kohgi, M. Itoh, H. Iwasa, N. Watanabe, S. Ikeda, and Y. Endoh (unpublished).
[28] U. Steigenberger, M. Hagen, R. Caciuffo, C. Petrillo, F. Cilloco, and F. Sacchetti, Nucl. Instrum. Methods Phys. Res. B **53**, 87 (1991); M. J. Bull, M. J. Harris, U. Steigenberger, M. Hagen, C. Petrillo, and F. Sacchetti, Physica B **234-236**, 1061 (1997).
[29] R. E. Watson and A. J. Freeman, Acta Crystallogr. **14**, 27 (1961).
[30] T. G. Perring, Ph.D. thesis, University of Cambridge, 1991.
[31] M. J. Cooper and R. Nathans, Acta Crystallogr. **23**, 357 (1967).
[32] S. A. Werner and R. Pynn, J. Appl. Phys. **42**, 4736 (1971).
[33] S. Yamamoto, Phys. Rev. Lett. **75**, 3348 (1995).
[34] J. Deisz, M. Jarrel, and D. L. Cox, Phys. Rev. B **48**, 10 227 (1993).